American Mineralogist, Volume 102, pages 2457–2466, 2017

The solubility of $CePO_4$ monazite and YPO_4 xenotime in KCl-H_2O fluids at 800 °C and 1.0 GPa: Implications for REE transport in high-grade crustal fluids

Philipp Mair[1,*], Peter Tropper[1], Daniel E. Harlov[2,3], and Craig E. Manning[4]

[1]Institute of Mineralogy and Petrography, Faculty of Geo- and Atmospheric Sciences, University of Innsbruck, Innrain 52f, A-6020 Innsbruck, Austria
[2]Helmholtz Zentrum Potsdam, Deutsches GeoForschungsZentrum, Telegrafenberg, D-14473 Potsdam, Germany
[3]Department of Geology, University of Johannesburg, P.O. Box 524, Auckland Park 2006, South Africa
[4]Department of Earth and Space Sciences, University of California, Los Angeles, California 90095-1567, U.S.A.

Abstract

Monazite ($CePO_4$) and xenotime (YPO_4) are important hosts for REE and thus can be used to monitor REE mass transfer in various settings. In this investigation, the solubilities of synthetic monazite and xenotime were measured in KCl-H_2O fluids at 800 °C and 1.0 GPa, using the piston-cylinder apparatus. The experimental results indicate an increase in monazite and xenotime solubility in aqueous fluids with moderate KCl mole fractions (X_{KCl}) in agreement with previous investigations of the solubility of these phases in NaCl-H_2O. Under all conditions, monazite and xenotime dissolve congruently. The solubility of synthetic monazite increases from 8 ppm in pure H_2O to 335 ppm at X_{KCl} = 0.506. The solubility of synthetic xenotime rises from 46 ppm in pure H_2O to 126 ppm at X_{KCl} = 0.348, above which it is constant or declines slightly. Monazite and xenotime solubilities are considerably lower in KCl-H_2O than in NaCl-H_2O at the same salt concentration. Best-fit equations for the solubilities of the two phases are:

$$c_{mz} = -464\, X_{KCl}^2 + 891\, X_{KCl} + 8$$

and

$$c_{xt} = -563\, X_{KCl}^2 + 432\, X_{KCl} + 46$$

where mz and xt stand for monazite and xenotime, and $X_{KCl} = n_{KCl}/(n_{KCl} + n_{H_2O})$ where n is moles. The change in solubilities with KCl implies that Ce dissolves as an anhydrous chloride complex ($CeCl_3$), whereas Y forms a mixed Cl-OH solute [$YCl(OH)_2$]. The data also imply that H_2O-NaCl fluids and H_2O-KCl fluids close to neutral pH can transport substantial amounts of REE and Y, thus obviating the need to invoke low-pH solutions in high-grade environments where they are highly unlikely to occur.

Keywords: Monazite, xenotime, solubility, experimental petrology, REE mobility, metamorphic fluids, brines

Introduction

Aqueous fluids are responsible for substantial mass transfer in high-pressure (P) and -temperature (T) environments. Understanding the scale and magnitude of fluid-mediated compositional change is central to many studies of magmatic and metamorphic systems and ore deposits such as REE-enriched iron oxide-apatite deposits (cf. Harlov et al. 2016) or REE-enriched carbonatites (e.g., Yang et al. 2003). For example, lithologies transported to deep-crustal conditions along Barrovian *P-T* paths show evidence for significant compositional modification by metamorphic fluids (e.g., Ague 1994a, 1994b). Similarly, in subduction zones, slab devolatilization generates a fluid phase that is capable of major metasomatic activity (e.g., Manning 2004). *P-T* environments (e.g., Barrovian and granulite metamorphism and subduction zones) often record evidence of mobilization of elements that show very low solubility in H_2O, such as Al, Ti, and rare-earth elements (REE). Explanations may involve extremes in pH or complexing with halogens, alkalis, or both or polymerization with alkalis, Al, and Si (e.g., Manning 2004; Newton and Manning 2010; Tropper et al. 2011, 2013). Several observations point to the participation of brines in high-grade metamorphic processes. These include not only findings of alkali and alkaline-earth halides as daughter crystals in fluid inclusions, but also appreciable concentrations of Cl measured in minerals from high-grade rocks such as amphiboles, biotite, scapolite, and apatite, and direct observations on high-temperature halides present in the intergranular space in high-grade rocks (e.g., Aranovich et al. 2014). Saline fluids may also be important in subduction-zone metasomatism (Barnes et al. 2017; Keppler 2017).

Accessory minerals are minor in abundance, but can contain elements as major components (for example Ce in monazite and

* E-mail: philipp.mair@uibk.ac.at

0003-004X/17/0012–2457$05.00/DOI: http://dx.doi.org/10.2138/am-2017-6172

Y in xenotime), which with respect to the whole rock would be considered trace elements. If these minerals are part of the solid assemblage, their solubility will govern the abundance of key trace elements in coexisting fluids, including Ti, Nb, Ta, Zr, Hf, and REE. Therefore knowledge of rare earth element (Y+REE) redistribution during high-grade metamorphism is of fundamental importance in determining the origin of typical light (L)REE-enrichment of calc-alkaline magmas, commonly ascribed to the metasomatic effects of a subducting slab on the overlying mantle wedge (e.g., Ionov and Hofmann 1995; Rubatto and Hermann 2003; Gao et al. 2007). It is therefore essential to understand the behavior of (Y+REE) carriers such as monazite and xenotime during that metasomatic processes that attend high-grade metamorphism and subduction.

Monazite and xenotime are important accessory phases in metamorphic and igneous rocks (e.g., Spear and Pyle 2002). Occurring over a range of metamorphic lithologies, settings, and *P-T* conditions, these phosphates have great utility as prograde index minerals that can be used for geochronology (e.g., Harrison et al. 2002) and geothermometry (e.g., Gratz and Heinrich 1997; Janots et al. 2008). They represent important reservoirs for light (LREE) and heavy (Y+HREE) rare earth elements. The exchange of (Y+REE) between orthophosphates and silicates, such as garnet, provides information concerning the *P-T* history of metamorphic terranes (e.g., Spear and Pyle 2002). Y+REE orthophosphates also play an important role in controlling the distribution of (Y+REE), U, and Th during granitoid crystallization (e.g., Montel 1993). Their high durability and resistance to metamictization make the (Y+REE) phosphates potential hosts for nuclear waste disposal (e.g., Ewing 2001). The mobility of REE in crustal and mantle fluids are especially important because of their role in REE ore-deposit formation (e.g., Williams-Jones et al. 2012; Harlov et al. 2016) as well as their contribution in tracing magmatic (e.g., Markl and Piazolo 1998; Agangi et al. 2010) and metamorphic (e.g., Yardley 1985; Brennan 1993) petrogenetic processes.

Potassium metasomatism has been recognized by field workers in high-grade metamorphic terranes for over a century (e.g., Billings 1938). Alkali exchange in natural feldspars (K-feldspathization) gives rise to "replacement antiperthite," a common texture in high-grade gneisses (Todd and Evans 1994; Hansen et al. 1995). Potassium species are also important constituents of high-grade metamorphic fluids (e.g., Aranovich and Newton 1997; Newton et al. 1998; Harlov and Förster 2002; Harlov 2012) and potassium metasomatism has been recognized in high-grade metamorphic terranes (e.g., Hansen et al. 1995; Newton et al. 1998; Harlov et al. 1998; Harlov and Förster 2002; Harlov 2012). KCl brines or K-rich also act as metasomatic fluids in xenoliths from the lower crust and upper mantle (Harlow and Davies 2004), kimberlites (Kamenetsky et al. 2004), as well as brine-rich inclusions in diamonds (Tomlinson et al. 2004). Sylvite (KCl) has been identified as a daughter mineral in some of the concentrated brine inclusions that have been described with increasing frequency in many petrogenetic settings, including granites (Dunbar et al. 1996), gabbros (Pasteris et al. 1995), high-grade gneisses (Touret 1985), carbonatites (Sampson et al. 1995), eclogites (Philippot and Selverstone 1991), and the super-high-pressure coesite-bearing metasediments (Philippot et al. 1995). KCl is thought to have been a major solute of the complex saline fluids that produced regional metasomatism and metal ore segregation in Cloncurry, Queensland (DeJong and Williams 1995) and the Melones Fault Zone of California (Albino 1995). The role of KCl-NaCl-H_2O-rich fluids has also been investigated in several experimental studies on the relationship between activity and concentration (Aranovich and Newton 1997), the stability of phlogopite (Aranovich and Newton 1998), fluid-induced dehydration of tonalites (Harlov 2004; Harlov et al. 2006) and biotite-amphibole gneiss (Safonov et al. 2012), monazite/apatite dissolution-reprecipitation (Harlov and Förster 2003; Harlov et al. 2005), quartz solubility (Shmulovich et al. 2005), and brine-assisted anataxis (Aranovich et al. 2014).

Despite their importance as minerals whose occurrence as prograde index minerals can be coupled with geochronology (e.g., Janots et al. 2009) and their economic importance (Williams-Jones et al. 2012; Harlov et al. 2016), little is known about the solubility systematics of two of the most important orthophosphate REE-bearing minerals, monazite ($CePO_4$-) and xenotime (YPO_4-), in aqueous fluids of various compositions at high *P* (>0.5 GPa) and *T* (>300 °C). It is therefore essential to understand their solubility behavior with respect to *P-T-*X_i conditions and complexation during metasomatic processes that attend high-grade crustal metamorphism and crustal/mantle/rock-fluid interactions occurring during subduction.

Experimental methods

Solubility experiments involving solutions with varying concentrations of KCl were conducted on synthetic crystals of monazite ($CePO_4$) and xenotime (YPO_4), and natural monazite from a beach sand in Cleveland Co., North Carolina (UCLA mineral collection MS 1762), which contains 59.96 wt% LREE (29.41 wt% Ce_2O_3, 13.44 wt% La_2O_3, 11.15 wt% Nd_2O_3, 3.08 wt% Pr_2O_3, 1.87 wt% Sm_2O_3 and 1.01 wt% Gd_2O_3) and 0.76 wt% HREE (with 0.55 wt% Y_2O_3, 0.08 wt% Dy_2O_3, 0.07 wt% Tb_2O_3, 0.02 wt% Ho_2O_3, 0.02 wt% Er_2O_3, and 0.02 wt% Yb_2O_3) (Tropper et al. 2011).

Synthetic crystals of monazite ($CePO_4$) or xenotime (YPO_4) were synthesized by mixing stoichiometric amounts of $REE(NO_3)\cdot 6H_2O$ and $(NH_4)_2HPO_4$ in solution. The resulting precipitate was allowed to settle and the excess fluid poured off. The precipitate was then dried and ground. Twenty grams of Pb-free flux (Na_2CO_3:MoO_3 = 1:3) mixed with 0.8 g precipitate was packed in a Pt crucible with a loose cover and heated to 1280 °C. The molten flux was allowed to equilibrate at 1280 °C for 15 h, and then cooled to 870 °C at 3 °C/h (Cherniak et al. 2004; Tropper et al. 2011). The resulting transparent, light brownish yellow, euhedral to semi-euhedral monazite and xenotime crystals range from 0.1 to 2 mm in diameter. The smaller crystals are inclusion-free, but some of the larger crystals (>1 mm) contain scattered melt inclusions.

Single crystals, optically free of flux melt inclusions, were selected for use in the solubility studies. Each crystal was first ground into spherical shapes with a diameter of ~1–2 mm using 400-grit emery paper to remove sharp edges, and then rolled in 800-grit emery paper until they acquired a polish. The polished crystals were cleaned in ethanol in an ultrasonic bath, and then dried at 120 °C for 15 min. This procedure generated single crystals that ranged in weight from 0.7 to 3.0 mg (Table 1). Each experiment consisted of an outer Pt capsule (outer diameter: 3.0 mm, thickness: 0.2 mm) and an inner Pt capsule (outer diameter: 2.0 mm, thickness: 0.1 mm) in which the monazite or xenotime single crystal was placed. Thick-walled Pt (0.2 mm) was used for the outer capsule to minimize puncturing by the thermocouple. The use of an inner capsule protected the crystal and minimized thermal gradients in the capsule (Tropper and Manning 2005). After inserting the crystal, the inner capsule was lightly crimped to facilitate H_2O penetration while ensuring crystal containment during the experiments. The inner Pt capsule, plus precisely weighed quantities of KCl and H_2O (Table 1), were then placed in the outer Pt capsule. The outer Pt capsule was sealed by arc-welding and then placed in a 120 °C oven for 30 min to check for leakage.

All experiments were performed at 800 °C and 1000 MPa in a non-end-loaded piston-cylinder apparatus, using 22 mm diameter NaCl assemblies with a cylindrical

graphite oven and sealed by pyrophyllite rings. Each double capsule assembly was placed horizontally at the center of the NaCl assembly surrounded by the graphite-furnace and packed in NaCl. It was covered with a small, thin pyrophyllite sheet to help prevent puncture by the thermocouple, which is in direct contact with the Pt capsule. Pressure and temperature was monitored using a pressure gauge and a NiCr-Ni thermocouple, respectively. Pressure was maintained to within 200 bar gauge pressure and the accuracy of the reported temperature is estimated to be ±2 °C. Each experiment was initially brought to 0.2 GPa and 100 °C and held for 15 min, then brought to 800 °C and 1.0 GPa following a temperature and pressure ramp of 20 °C/min and 0.02 GPa/min. After 12 h, the experiments were quenched to $T < 150$ °C and $P < 0.6$ GPa within several seconds by shutting off the power to the graphite oven. Run times of 12 h for each experiment at 800 °C and 1.0 GPa were assumed sufficient to ensure significant reaction and equilibration of the monazite or xenotime starting crystals with the solution. Attainment of constant solubility within 12 h is consistent with equilibration rates in other solubility measurements at high T and P, based on previous studies (e.g., Caciagli and Manning 2003; Tropper and Manning 2005; Tropper et al. 2011).

After each experiment, the outer capsule was pierced with a needle, and the pH of the quench fluid was checked with a pH-indicator paper with an accuracy of <0.5 pH units (Table 1). After drying for 30 min at 120 °C, the monazite or xenotime crystal was then extracted from the inner capsule, treated ultrasonically in ethanol to remove adhering quench precipitate, dried at 120 °C, and weighed with a Mettler Toledo XP2U ultra-microbalance (1σ = 0.1 μg) (Table 1). All monazite and xenotime grains were then examined optically with a binocular microscope. Single crystals from selected experiments were mounted onto double-sided carbon tape and characterized by a JEOL JSM-6010LV scanning electron microscope (SEM) equipped with a Quantax EDS (Bruker).

The solubility of monazite and xenotime is reported in parts per million by weight (ppm), and is calculated via the formulas $(\Delta m_{mz}/H_2O + KCl + \Delta m_{mz})\times10^6$ and $(\Delta m_{xt}/H_2O + KCl + \Delta m_{xt})\times10^6$, where mz and xt stand for monazite and xenotime. Reported mole fractions of KCl (X_{KCl}) were calculated from the starting ratio $n_{KCl}/(n_{KCl} + n_{H_2O})$ in the experiment. KCl and H_2O masses were determined on a Mettler Toledo AX205 DeltaRange microbalance (1σ = 0.03 mg) (Table 1). For further speciation calculations the monazite and xenotime mass loss (Δm_{mz} and Δm_{xt}) and the measured pH were used to calculate ionic species utilizing the concept of the limiting reactant (Tables 2a and 2b).

Results

Textures and equilibrium

The experimental results are given in Table 1. Run products included partly dissolved starting monazite (Fig. 1a) and xenotime crystals (Fig. 1c), recrystallized $CePO_4$ grains on the surface of monazite starting crystals (Fig. 1b), yttrium chloride crystals on the surface of xenotime starting crystals (Fig. 1d), newly formed secondary monazite (Figs. 2a and 2b), xenotime (Figs. 2c and 2d), and yttrium chloride crystals (Fig. 2c) in the outer capsules of some experiments, and a sub-micrometer-sized white powder consisting of KCl (Fig. 2). The chemical identification of the yttrium chloride crystals was done semi-quantitatively

Table 1. Experimental results in the system monazite-H_2O-KCl and xenotime-H_2O-KCl at 800 °C and 1.0 GPa

Run number	Time (h)	H_2O in (mg)	KCl in (mg)	X_{KCl}	Crystal in (mg)	Crystal out (mg)	Solubility (ppm)	pH
			Synthetic monazite (H_2O-KCl)					
Mnz-18*	90	35.89	0.00	0.000	1.1635	1.1632	8	–
Mnz_003	12	35.20	16.44	0.101	2.8190	2.8150	78 (4)	7.0
Mnz_005	12	31.01	23.11	0.153	2.6666	2.6603	116 (2)	7.0
Mnz_013	12	21.77	31.44	0.259	1.3995	1.3872	232 (6)	7.5
Mnz_012	12	14.08	38.07	0.395	1.6765	1.6615	288 (8)	7.0
Mnz_015	12	9.08	38.50	0.506	1.0983	1.0823	335 (3)	7.5
			Natural monazite (H_2O-KCl)					
Mnz_017	12	21.31	31.38	0.262	1.2343	1.2245	186 (3)	8.0
			Synthetic xenotime (H_2O-KCl)					
Xnt-4*	12	41.62	0.00	0.000	2.3541	2.3522	46	–
Xnt_023	12	34.60	15.81	0.099	0.8727	0.8693	67 (5)	7.0
Xnt_024	12	25.59	27.31	0.205	0.9871	0.9805	124 (1)	7.5
Xnt_028	12	16.31	36.07	0.348	0.9329	0.9263	126 (4)	7.5
Xnt_027	12	10.47	42.17	0.493	0.7068	0.7004	122 (5)	7.5

Notes: Explanation of "Crystal in" and "Crystal out" refers, respectively, to the weights before and after the experiment. Weights reported to two decimal places were determined on a Mettler Toledo AX205 DeltaRange microbalance (1σ = 0.03 mg); those to four places were determined on a Mettler Toledo XP2U ultra microbalance (1σ = 0.1 μg). The solubility is expressed with the 1σ uncertainty, based on propagation of weighing errors. Run numbers Mnz-18 and Xnt-4, which are marked with an asterisk, are the experiments in pure H_2O at 800 °C and 1.0 GPa from Tropper et al. (2011).

Table 2a. Chemical reaction model of the system monazite-H_2O-KCl

	Monazite-KCl								
	1 $CePO_4$ + 3 KCl =				1 $CeCl_3$ + 1 K_3PO_4				
Run number	Δm $CePO_4$ (μg)	m H_2O (mg)	m KCl (mg)	X_{KCl}	m $CeCl_3$ (μg)	m K_3PO_4 (μg)	m H_2O rest (mg)	m KCl rest (mg)	obs pH
Mnz_003	4.05	35.20	16.440	0.101	4.25	3.66	35.20	16.436	7.0
Mnz_013	12.35	21.77	31.440	0.259	12.95	11.15	21.77	31.428	7.5
Mnz_015	15.98	9.08	38.503	0.506	16.75	14.42	9.08	38.487	7.5

Notes: Based on the limiting reactant approach for monazite, the dissolution reaction 1 $CePO_4$ + 3 KCl = 1 $CeCl_3$ + 1 K_3PO_4 occurs over the investigated range of X_{KCl} (0.101–0.506) and implies no interaction with H_2O. The amount of water remains unchanged before and after the chemical reaction (m H_2O = m H_2O rest).

Table 2b. Chemical reaction model of the system xenotime-H_2O-KCl

	Xenotime-H_2O =-KCl										
	1 YPO_4 + 4 H_2O + 3 KCl =				1 $YCl(OH)_2$ + 1 KH_2PO_4 + 2 HCl + 2 KOH						
Run number	Δm YPO_4 (μg)	m H_2O (mg)	m KCl (mg)	X_{KCl}	m $YCl(OH)_2$ (μg)	m KH_2PO_4 (μg)	m HCl (μg)	m (KOH) (μg)	m H_2O rest (mg)	m KCl rest (mg)	obs pH
Xnt_028	6.60	16.310	36.070	0.348	5.68	4.88	2.62	4.03	16.307	36.062	7.5
Xnt_027	6.40	10.468	35.500	0.493	5.51	4.74	2.54	3.91	10.465	35.492	7.5

Notes: Based on the limiting reactant approach for xenotime, the dissolution reaction 1 YPO_4 + 4 H_2O + 3 KCl = 1 $YCl(OH)_2$ + 1 KH_2PO_4 + 2 HCl + 2 KOH occurs over the investigated range of X_{KCl} (0.35–0.45) and implies an interaction with KCl and H_2O. The corresponding amounts of water and salt change accordingly after the chemical reaction (m H_2O > m H_2O rest and m KCl > m KCl rest).

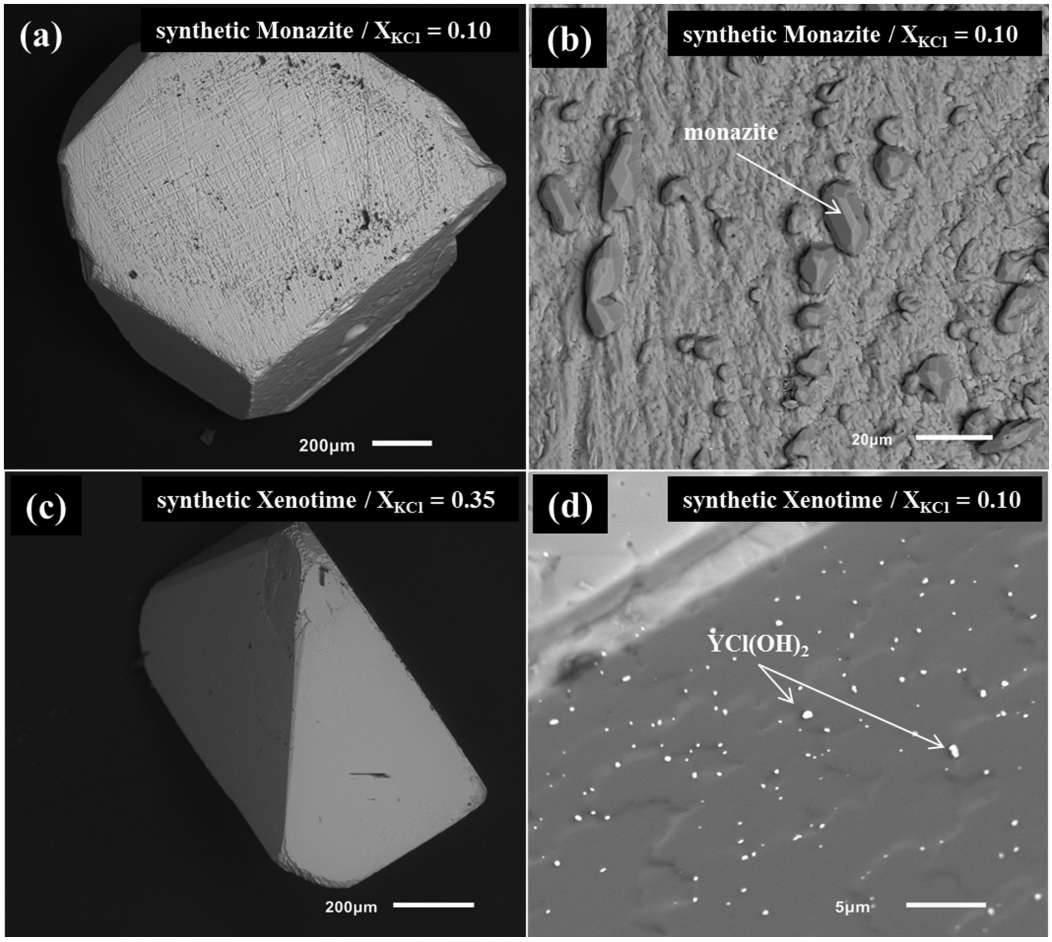

FIGURE 1. SEM images of run products from selected experiments. (**a**) $CePO_4$ crystal after dissolution at X_{KCl} = 0.101 (Mnz_003). (**b**) Surface of the $CePO_4$ crystal dissolved in X_{KCl} = 0.101, displaying dissolution grooves and recrystallization. (**c**) YPO_4 crystal after dissoultion at X_{KCl} = 0.348 (Xnt_028). (**d**) YPO_4 crystal after dissolution in X_{KCl} = 0.099 (Xnt_023) fluid, with tiny quench crystals [$YCl(OH)_2$] adhering to the surface.

using EDS analysis on the scanning electron microscope (SEM). Despite the small grain size and their adherence to the crystal faces of the starting crystals EDS analysis showed distinct Y and Cl peaks only and based on the approximate ratio between Y and Cl of 1:1, we infer the stoichiometry of this compound to be $YCl(OH)_2$. This quench phase most likely formed from the strongly hygroscopic phase YCl_3, which reacts directly with H_2O to $YCl(OH)_2$ and HCl based on the following chemical reaction: 1 YCl_3 + 2 H_2O = 1 $YCl(OH)_2$ + 2 HCl (Klevtsova and Klevtsov 1965; Haschke 1974; Zhuravleva et al. 2013). Tropper et al. (2011) postulated for the system xenotime-H_2O-NaCl that a similar simple equilibrium could account for this relationship namely: YPO_4 + NaCl + 2 H_2O = $YCl(OH)_2$ + NaH_2PO_4. The residual monazite and xenotime crystals displayed solution-rounded edges (Figs. 1a and 1c) and in some cases, significant dissolution grooves (Fig. 1a). The recrystallized $CePO_4$ grains on the surface of the monazite starting crystals occur as idiomorphic, prismatic, tabular-granular aggregates (Fig. 1b) and quench crystals occur as tiny, round precipitates, which were distributed randomly on the surface of the xenotime starting crystals (Fig. 1d). The newly formed euhedral secondary monazite and xenotime crystals occur as hollow, prismatic needles (Fig. 2), which are randomly distributed throughout the inner and outer capsules. The abundance of secondary monazite and xenotime needles increased with increasing X_{KCl}, accompanied by an increase in monazite or xenotime solubility (Table 1). The size of the secondary monazite crystals was up to ~15 µm along the *c*-axis (Figs. 2a and 2b), the size of the secondary xenotime crystals was up to ~5 µm along the *c*-axis (Figs. 2c and 2d). Both secondary monazite and xenotime crystals vary from sparse and separate crystallites to fibrous aggregates that were mostly embedded in KCl aggregates (Fig. 2). Two generations of secondary monazite quench crystals with different size and morphology (Fig. 2b) were found in the system monazite-H_2O-KCl at a mole fraction of X_{KCl} = 0.1. The first generation of monazites (sec mz I) can be recognized by its characteristic prismatic crystals (Figs. 2a and 2b). The second generation of monazites (sec mz II) occurs as stellate clusters of thin needles, which are significantly smaller than the monazite crystals of the first generation. In addition to the secondary monazite and xenotime crystals, <2 µm tabular-prismatic grains of $YCl(OH)_2$ crystals were observed in the system xenotime-H_2O-KCl at a mole fraction of X_{KCl} = 0.1,

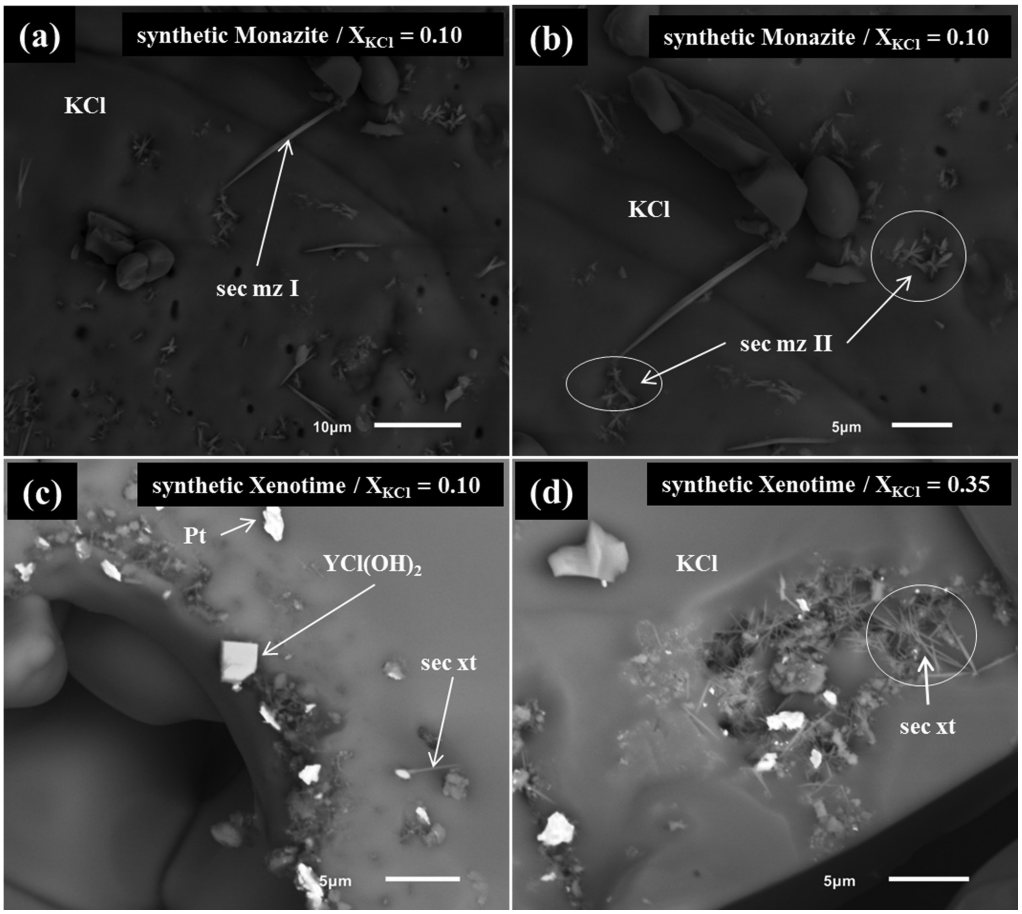

FIGURE 2. SEM images of the quench material from selected experiments. (**a** and **b**) Two generations of secondary monazite crystals, that occur as prismatic needles (sec mz I) and stellate clusters (sec mz II), which nucleated in the outer casule upon quench and embedded in KCl aggregates. (**c** and **d**) Tabular–prismatic crystal of $YCl(OH)_2$ and secondary xenotime crystals (sec xt), which embedded in KCl aggregates.

embedded in KCl aggregates (Fig. 2c).

Based on the textural observations, it can be assumed that the newly formed secondary monazite, xenotime, and yttrium chloride crystals nucleated and grew during quenching to room temperature from the experimental *T*, whereas the KCl aggregates precipitated during drying after initial puncturing of the outer capsule. The attribution of these secondary phases as quench material is in accordance with previous observations from similar experiments (e.g., Tropper and Manning 2005, 2007a, 2007b; Antignano and Manning 2008; Tropper et al. 2011). No evidence for vapor-transport of monazite or xenotime was observed, unlike in some mineral-fluid systems such as calcite, rutile, and corundum (Caciagli and Manning 2003; Tropper and Manning 2005, 2007b) or fluorapatite in the system NaCl + H_2O (Antignano and Manning 2008).

Monazite solubility in H_2O-KCl

The experimental results in the system monazite-H_2O-KCl are given in Table 1 and shown in Figure 3a. At 800 °C and 1.0 GPa, the solubility of the synthetic monazite in pure H_2O is 8 ppm (Table 1) (Tropper et al. 2011). The solubilities of synthetic monazite in H_2O-KCl fluids indicate an increase in the dissolved monazite concentration with rising X_{KCl} from 78 ± 4 ppm (X_{KCl} = 0.101) to 335 ± 3 ppm (X_{KCl} = 0.506; Table 1). The data on the variation in synthetic monazite solubility with X_{KCl} at 1.0 GPa and 800 °C (Fig. 3a) can be fit to a second-degree polynomial function using least-squares regression:

$$c_{mz} = -464\, X_{KCl}^2 + 891\, X_{KCl} + 8 \quad (1)$$

where c_{mz} Is the solubility of the synthetic monazite in parts per million (R^2 = 0.986) and X_{KCl} is the mole fraction of KCl. It can be also seen from Figure 3a that at X_{KCl} = 0.262, the solubility of natural monazite (186 ± 3 ppm) (Table 1) fits well to the data of synthetic monazite solubility. In contrast to the H_2O-KCl system, monazite solubilities are considerably higher in the H_2O-NaCl system as shown by Tropper et al. (2011). Their results also indicate an increase in the dissolved monazite concentration with rising X_{NaCl} to near halite saturation from 152 ppm (X_{NaCl} = 0.092) to 442 ppm (X_{NaCl} = 0.498) (Fig. 3a). The increase in the $CePO_4$ solubility with increasing NaCl concentration is similar to that seen for apatite, fluorite, calcite, anhydrite (Antignano and Manning 2008; Tropper and Manning 2007a; Newton and Manning 2002, 2005), and monazite in the system H_2O-KCl. In

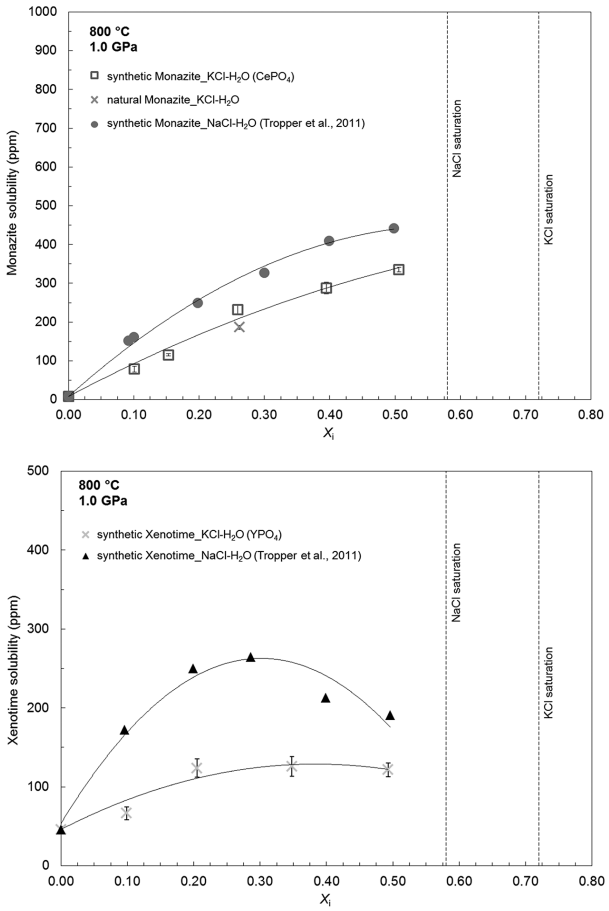

FIGURE 3. (**a**) Monazite solubility vs. the mole fraction of KCl and NaCl (X_i) at 800 °C and 1.0 GPa. The error bars are 2σ and are calculated based on the weighing uncertainties. The solid line in the system monazite-KCl-H_2O represents the fitted solubilities from Equation 1. Results of Tropper et al. (2011) from monazite-NaCl-H_2O at 800 °C and 1.0 GPa shown for comparison. Halite and sylvite saturation estimated from Aranovich and Newton (1996, 1997). (**b**) Xenotime solubility vs. the mole fraction of KCl and NaCl (X_i) at 800 °C and 1.0 GPa. The error bars are 2σ and are calculated based on the weighing uncertainties. The solid line in the system xenotime-KCl-H_2O represents the fitted solubilities from Equation 2. Results of Tropper et al. (2011) from xenotime-NaCl-H_2O at 800 °C and 1.0 GPa shown for comparison. Halite and sylvite saturation estimated from Aranovich and Newton (1996, 1997).

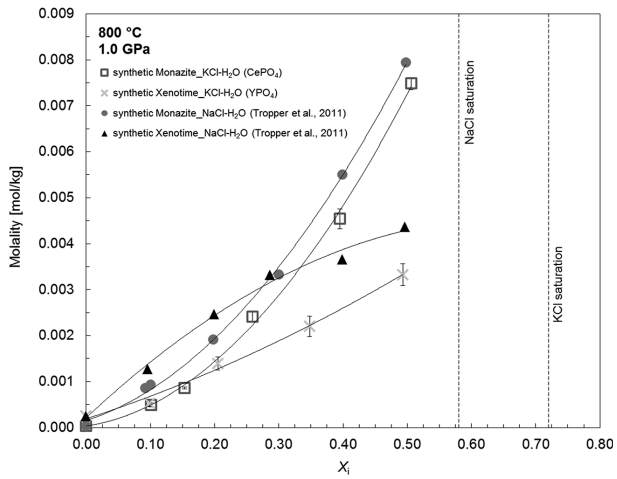

FIGURE 4. The relation between the molality of monazite and xenotime vs. the mole fraction of KCl and NaCl (X_i) at 800 °C and 1.0 GPa. Results of Tropper et al. (2011) from monazite and xenotime in the system NaCl-H_2O at 800 °C and 1.0 GPa are shown for comparison. Halite and sylvite saturation estimated from Aranovich and Newton (1996, 1997).

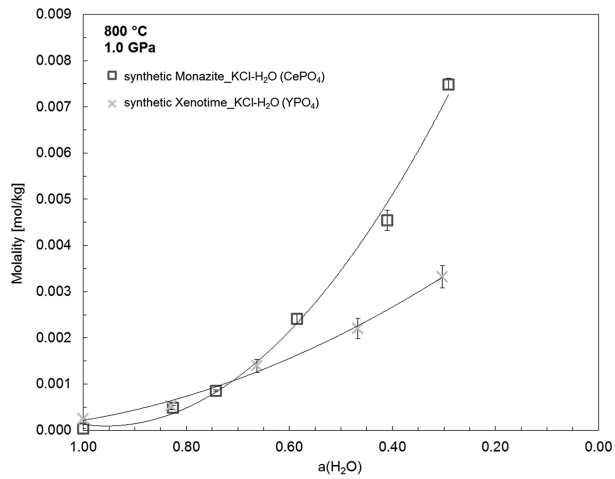

FIGURE 5. The relation between the molality of monazite and xenotime in the system H_2O-KCl vs. the activity of H_2O at 800 °C and 1.0 GPa.

addition, the quench pH of the aqueous solutions in the monazite-H_2O-KCl experiments was 7.0–7.5 (Table 1).

Figures 4 and 5 show the relationship between the molality of monazite vs. the mole fraction of KCl (X_{KCl}) and the activity of H_2O at 800 °C and 1.0 GPa. The molality of the monazite is reported in mol/kg, and is calculated from the amount of substance (n_{mz}) divided by the mass of H_2O+KCl. The H_2O and KCl activities were calculated using the Aranovich and Newton (1996, 1997) NaCl-KCl *a-X* formulation. Aranovich and Newton (1997) found that the KCl component lowers a_{H_2O} even more than NaCl at a given *T*, *P*, and X_{H_2O}, and that the KCl activity is lower for a given salt concentration than the NaCl activity (Aranovich and Newton 1996). At 1.0 GPa, the solutions closely approach an ideal fused salt mixture, where the activities of H_2O and KCl correspond to an ideal activity formulation. The low H_2O activity at high pressures in concentrated KCl solutions indicates that such solutions should be feasible as chemically active fluids capable of coexisting with solid rocks in many deep crustal and upper mantle metamorphic and metasomatic processes (Aranovich and Newton 1996).

Xenotime solubility in H_2O-KCl

The experimental results for the system xenotime-H_2O-KCl are given in Table 1 and shown in Figure 3b. In pure H_2O at 800 °C and 1.0 GPa, the solubility of synthetic xenotime is 46 ppm (Table 1) and is thus ~6 times higher than for synthetic monazite (8 ppm) (Table 1; Tropper et al. 2011). The solubili-

ties of synthetic xenotime in H_2O-KCl fluids show an increase in the dissolved xenotime concentration with X_{KCl} increasing from 67 ± 5 ppm (X_{KCl} = 0.099) to 126 ± 4 ppm (X_{KCl} = 0.348) (Table 1) (Fig. 3b). At X_{KCl} > 0.348 the solubility of xenotime decreases to 122 ± 5 ppm (X_{KCl} = 0.493) (Fig. 3b). The data can be fit using a second-degree polynomial function to describe the synthetic xenotime solubility as a function of X_{KCl} at 800 °C and 1.0 GPa (Fig. 3b):

$$c_{xt} = -563\, X_{KCl}^2 + 432\, X_{KCl} + 46 \quad (2)$$

where c_{xt} is the solubility of synthetic xenotime in parts per million (R^2 = 0.921) and X_{KCl} is the mole fraction of KCl. Again xenotime solubilities are considerably higher in the system H_2O-NaCl as shown by Tropper et al. (2011) where the dissolved xenotime concentration increases with rising X_{NaCl} from 173 ppm (X_{NaCl} = 0.096) to 265 ppm (X_{NaCl} = 0.286) (Fig. 3b). At X_{NaCl} > 0.286, the solubility decreases to 212 ppm (X_{NaCl} = 0.399) and 191 ppm (X_{NaCl} = 0.496) (Fig. 3b). YPO_4 solubility in the system H_2O-NaCl by Tropper et al. (2011) increases in a manner similar to that of corundum and wollastonite (Newton and Manning 2006), and shows a different trend than the solubility of YPO_4 in the system H_2O-KCl (Fig. 3b). Similar to the monazite-H_2O-KCl experiments, the xenotime-H_2O-KCl experiments have neutral quench pH values of 7–7.5 over the investigated X_{KCl} range (Table 1).

Figures 4 and 5 show the relationship between the molality of xenotime vs. the mole fraction of KCl (X_{KCl}) and the activity of H_2O at 800 °C and 1.0 GPa.

Discussion

The low solubility of monazite and xenotime in pure H_2O experimentally obtained by Tropper et al. (2011) makes it difficult to explain the natural association of these minerals with metasomatic features in igneous and metamorphic rocks, such as hydrothermal alteration assemblages, veins, and skarns (e.g., Gieré 1996). The fluid flux must be high enough to mobilize relatively insoluble REE in which the solubility of (Y+REE) orthophosphates is low in near-neutral pH aqueous fluids and increases in acidic fluids (e.g., Tropper et al. 2013). An alternative mechanism for the dissolution and transportation of orthophosphate components is a high NaCl and/or KCl concentration in the fluid phase. Tropper et al. (2011) found that YPO_4 solubility in pure H_2O at 800 °C and 1 GPa is greater (46 ppm) than that of $CePO_4$ (8 ppm). This is in nominal disagreement with the general observation that monazite is more common than xenotime in hydrothermal veins and other metasomatic features, which implies greater solubility of LREE relative to HREE and Y (e.g., Schmidt et al. 2007), and suggests that LREE are more abundant than HREE in such systems. However, REE and Y dissolution in natural fluids are controlled by ligands other than H_2O or phosphate, such as chloride, fluoride, and sulfate, all of which can be expected to occur in varying proportions (e.g., Williams-Jones et al. 2012). Consequently, experimental results obtained using pure H_2O only represent an end-member scenario unlikely to occur in nature.

To obtain information on the interaction of monazite and xenotime with pure H_2O and KCl+H_2O solutions, the following generalized dissolution reactions may be written (Newton and Manning 2006, 2010; Tropper et al. 2011):

$$n\ CePO_4 + a\ KCl + b\ H_2O = k \text{ solute species} \quad (3a)$$

or

$$n\ YPO_4 + a\ KCl + b\ H_2O = k \text{ solute species} \quad (4a)$$

where n are the number of moles of monazite or xenotime, and a and b are the number of moles of KCl and H_2O consumed to produce k moles of solutes per mole of orthophosphate dissolved. The k moles of solutes per mole of orthophosphate were calculated assuming complete dissociation. The dissociation is represented by the following equations (Aranovich and Newton 1996; Newton and Manning 2006):

$$n\ Ce^{3+} + n\ PO_4^{3-} + a\ K^+ + a\ Cl^- + b\ H^+ + b\ OH^- = k \quad (3b)$$

or

$$n\ Y^{3+} + n\ PO_4^{3-} + a\ K^+ + a\ Cl^- + b\ H^+ + b\ OH^- = k. \quad (4b)$$

The relative molar proportions of KCl and H_2O in Equations 3a and 4a were evaluated using the technique outlined in Newton and Manning (2006, 2010). In case that the solubility of monazite or xenotime decreases with X_{KCl}, then Ce^{3+} or Y^{3+} solutes would likely be hydrous species, and there would be no interaction with K^+ and/or Cl^-. Similarly, monotonic increase with X_{KCl} would imply no interaction with H^+ and/or OH^-. If monazite and xenotime solubility increases to a plateau-like maximum and then declines this would imply that their solutes include both hydrates and K and/or Cl complexes. Figures 6a and 6b shows the variations in the relative solubility enhancements of synthetic monazite and xenotime, expressed as a solute mole fraction for a given X_{KCl} relative to that in pure H_2O. The effect of KCl on monazite and xenotime solubility can be assessed from the log-ratios X_{mz}/X°_{mz} and X_{xt}/X°_{xt}, where X°_{mz} and X°_{xt} are the mole fractions of monazite and xenotime in pure H_2O. The ratio log X/X° thus represents the magnitude of solubility enhancement by a given KCl mole fraction.

Values of log X/X°, especially for synthetic monazite in KCl solutions, increase with increasing X_{KCl} over the investigated range and this implies that the activity of H_2O does not significantly influence monazite solubility (b = 0 in Eq. 3a). This and the positive dependence of solubility on the square of X_{KCl} (Eq. 1) suggests that 3 mol of KCl per mole of $CePO_4$ form anhydrous solute species upon dissolution (a = 3). A simple chemical equilibrium that could account for this relationship is:

$$1\ CePO_4 + 3\ KCl = 1\ CeCl_3 + 1\ K_3PO_4. \quad (5)$$

The observed dissolution products in the KCl-bearing fluids are newly formed secondary monazite (Figs. 2a and 2b), $CeCl_3$, and K_3PO_4 (Eq. 5). Tropper et al. (2011) postulated that for the system monazite-H_2O-NaCl a similar simple equilibrium could account for this relationship namely: $CePO_4 + 2\ NaCl = CeCl_2^+ + Na_2PO_4^-$. Table 2a represents a chemical reaction model of the system monazite-H_2O-KCl in which the quantified reaction products of $CeCl_3$ and K_3PO_4 are listed.

In contrast to monazite, the values of log X/X° for the synthetic xenotime are not sufficiently precise to define a maximum as

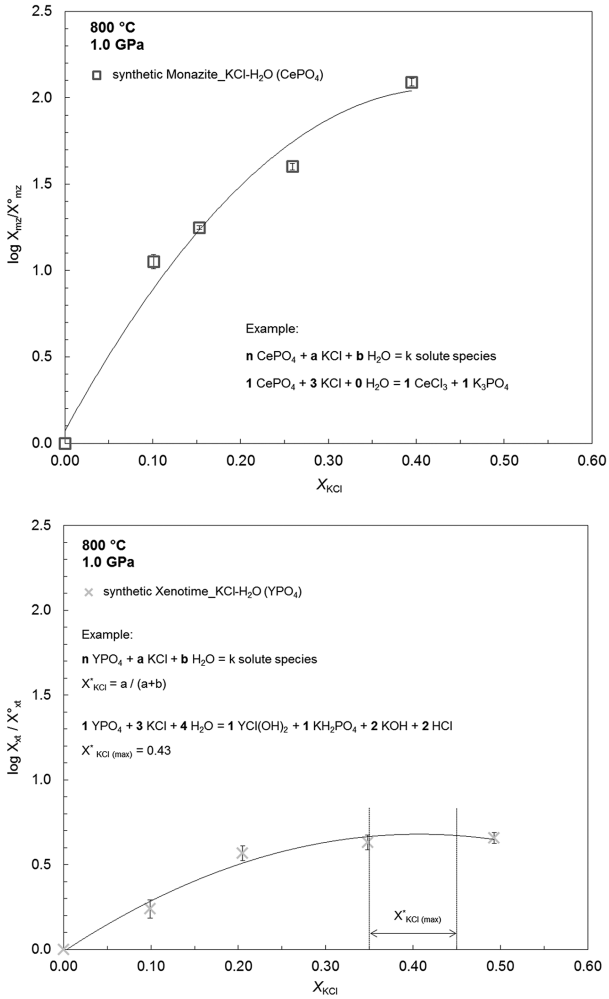

FIGURE 6. (**a**) Logarithm of the solubility enhancement of monazite, X_{mz}/X^{o}_{mz}, vs. X_{KCl} at 800 °C and 1.0 GPa. Values of log X_{mz}/X^{o}_{mz} Increase continuously with increasing X_{KCl} over the investigated range and this implies that the activity of H_2O does not significantly influence monazite solubility ($b = 0$). This suggests that 3 mol of KCl per mole of $CePO_4$ form anhydrous solute species upon dissolution ($a = 3$). (**b**) Logarithm of the solubility enhancement of xenotime, X_{xt}/X^{o}_{xt}, vs. X_{KCl} at 800 °C and 1.0 GPa. Values of X_{xt}/X^{o}_{xt} rise with increasing X_{KCl} over the investigated range to a maximum at X_{KCl} between 0.35 and 0.45. This implies that the activities of KCl and H_2O significantly influence xenotime solubility and that a (for KCl) is 3 and b (for H_2O) varies between 5.5 ($X_{KCl} = 0.35$) and 3.6 ($X_{KCl} = 0.45$).

in the NaCl system by Tropper et al. (2011). Nevertheless, the data rise with increasing X_{KCl} over the investigated range to a maximum at X_{KCl} between 0.35 and 0.45 (Fig. 6b). This implies that the activities of KCl and H_2O significantly influence xenotime solubility. Following the approach of Newton and Manning (2006), the KCl mole fraction, at which the maximum solubility occurs, defines the ratio of a to b in Equation 6 via:

$$\frac{-b \pm \sqrt{b^2 - 4ac}}{2a} \tag{6}$$

and implies that a (for KCl) is 3 and b (for H_2O) varies between 5.5 ($X_{KCl} = 0.35$) and 3.6 ($X_{KCl} = 0.45$) (Fig. 6b). A simple chemical equilibrium that could account for this relationship at $X_{KCl} = 0.43$ is:

$$1\ YPO_4 + 4\ H_2O + 3\ KCl = 1\ YCl(OH)_2 + 1\ KH_2PO_4 + 2\ KOH + 2\ HCl \tag{7}$$

where $a = 3$ and $b = 4$. The reaction products in the KCl-bearing fluids are $YCl(OH)_2$ (Figs. 1d and 2c), KH_2PO_4, KOH, and HCl (Eq. 7). The reverse reaction is defined as a neutralization reaction and occurs during the quenching process, in which the acid (HCl) and the base (KOH) react to form H_2O and KCl and the H^+ combines with OH^- to generate H_2O. This results in a quench pH equal to 7.

The dissolution products proposed in Equations 5 and 7 suggest that, in NaCl and also KCl-bearing fluids with neutral pH, the degree of Cl coordination for Y is lower than for Ce (Tropper et al. 2011). Assuming similar geochemical behavior for Y and REE, this is consistent with the steric hindrance of chloride complexation with HREE relative to LREE proposed by Mayanovic et al. (2009). The common occurrence of NaCl and KCl-rich fluids in crustal and mantle settings (e.g., Newton et al. 1998; Yardley and Graham 2002; Newton and Manning 2010) could offer a simple mechanism to explain numerous cases of LREE mobility. Table 2b represents a chemical reaction model for the system xenotime-H_2O-KCl, in which the quantified reaction products of $YCl(OH)_2$ and KH_2PO_4 are listed.

IMPLICATIONS

Field studies of high-grade rocks show that the mobility of REE and Y in granulite-facies terranes is greatly enhanced in the presence of brines (e.g., Newton et al. 1998; Harlov 2011; Aranovich et al. 2014) because brine-bearing fluid inclusions have been observed in granulites (e.g., Markl et al. 1998). It, therefore, has been proposed that REE (and, by extension, Y) mobility may be enhanced by dissolved halogens in some cases as highly concentrated brines (e.g., Pan and Fleet 1996; Schmidt et al. 2007; Antignano and Manning 2008; Newton and Manning 2010; Tropper et al. 2011, 2013). KCl brines or K-rich fluids in the lower crust and upper mantle, because of their high mechanical mobility and alkali-exchanging potential, are feasible metasomatic fluids for various high-grade rocks (Hansen et al. 1995; Newton et al. 1998; Harlov et al. 1998; Harlov and Förster 2002). Field observations (e.g., Touret and Nijland 2013) and experimental investigations (Harlov 2004) have demonstrated that a typical metasomatic feature associated with the presence of a high-salinity low-H_2O activity fluid is the presence of K-feldspar veining along the grain boundaries of minerals such as quartz, biotite, and plagioclase. Tropper et al. (2011) experimentally determined the solubility of $CePO_4$ monazite and YPO_4 xenotime in H_2O–NaCl solutions at 800 °C and 10 kbar. Their results indicate that the solubility of both Ce and Y increase with rising X_{NaCl}. Moreover, it has been shown that the most saline solutions exhibit a strong preference for LREE over HREE (Reed et al. 2000) and additional experiments in the system NaF-H_2O by Tropper et al. (2013) found that NaF solutions yielded an even stronger increase in Ce/Y concentration with rising salt concentrations. The present experiments in the system KCl-H_2O strongly corroborate the NaCl-H_2O experiments

although the extent of solubility is lower. These experimental results help to explain key features of REE geochemistry in high-grade metamorphic processes since brine-induced anatexis will result in a noticeable depletion in the bulk REE concentration compared to parental rocks without the presence of brines as well as a decrease in the LREE/HREE ratio in the residual rock from which the melt was extracted.

Another important aspect is large-scale metasomatism involving brines. Metasomatic alteration is conjectured to involve infiltrating NaCl and KCl-bearing brines during peak metamorphism as well as post peak and possibly more H_2O-rich fluids during uplift and cooling. Alkali-halide brines play an important role in mass transport (e.g., K-metasomatism) and mineral-fluid-melt phase equilibria in the lower crust (e.g., Newton et al. 1998; Yardley and Graham 2002; Harlov and Förster 2002; Newton and Manning 2010). With respect to the formation of large-scale ore deposits the experimental results by Harlov et al. (2002), Taghipour et al. (2015), and Harlov et al. (2016) also support the extensive metasomatic alteration and remobilization of REE-enriched iron-oxide-apatite (IOA) deposits due to the presence of brine-rich fluids. This fact is corroborated by several experiments, which have shown that the formation of monazite and xenotime associated with apatite is a metasomatically induced process that results from the interaction of brine-rich fluids that are reactive with the (Y+REE)-bearing apatite (Harlov et al. 2002, 2005, 2016; Harlov and Förster 2003; Harlov 2015). These examples clearly show that further experimental investigations are still needed to understand the behavior of (Y+REE) carriers such as monazite and xenotime in the presence of brine-rich fluids, which frequently accompany high-grade metamorphism and metasomatic processes.

Acknowledgments

The financial support from the Institute of Mineralogy and Petrography, University of Innsbruck is greatly acknowledged. Martina Tribus is thanked for her help with the SEM and Hannes Witting for his help in the high-pressure laboratory. Craig E. Manning was supported by U.S. National Science Foundation grant EAR 1347987. The manuscript was significantly improved by reviews by Anselm Loges, and an anonymous reviewer. Don Baker is gratefully acknowledged for the editorial handling of the manuscript.

References cited

Agangi, A., Kamenetsky, V.S., and McPhie, J. (2010) The role of fluorine in the concentration and transportation of lithophile trace lements in felsic magmas: insights from the Gawler Range Volcanics, South Australia. Chemical Geology, 273, 314–325.

Ague, J.J. (1994a) Mass-transfer during Barrovian metamorphism of pelites, south-central Connecticut. 1. evidence for changes in composition and volume. American Journal of Science, 294, 1039–1057.

——— (1994b) Mass-transfer during Barrovian metamorphism of pelites, south-central Connecticut. 2. channelized fluid-flow and the growth of staurolite and kyanite. American Journal of Science, 294, 1061–1134.

Albino, G.V. (1995) Sodium metasomatism along the Melones Fault Zone, Sierra Nevada Foothills, California, USA. Mineralogical Magazine, 59, 383–400.

Antignano, A., and Manning, C.E. (2008) Fluorapatite solubility in H_2O and H_2O-NaCl at 700 to 900°C and 0.7 to 2.0 GPa. Chemical Geology, 251, 112–119.

Aranovich, L.Y., and Newton, R.C. (1996) H_2O activity in concentrated NaCl solutions at high pressures and temperatures measured by the brucite-periclase equilibrium. Contributions to Mineralogy and Petrology, 125, 200–212.

——— (1997) H_2O activity in concentrated KCl and KCl-NaCl solutions at high temperatures and pressures measured by the brucite-periclase equilibrium. Contributions to Mineralogy and Petrology, 127, 261–271.

——— (1998) Reversed determination of the reaction: Phlogopite + quartz = enstatite + potassium feldspar + H_2O in the ranges 750–875 °C and 2–12 kbar at low H_2O activity with concentrated KCl solutions. American Mineralogist, 83, 193–204.

Aranovich, L.Y., Makhluf, A.R., Manning, C.E., and Newton, R.C. (2014) Dehydration melting and the relationship between granites and granulites. Precambrian Research, 253, 26–37.

Barnes, J.D., Manning, C.E., Scambelluri, M., and Selverstone, J. (2017) The behavior of halogens during subduction-zone processes. In D. Harlov and L.Y. Aranovich, Eds., The Role of Halogens in Terrestrial and Extraterrestrial Geochemical Processes. Springer, in press, DOI: 10.1007/978-3-319-61667-4.

Billings, M.P. (1938) Introduction of potash during regional metamorphism in western New Hampshire. Geological Society of America Bulletin, 49, 289–302.

Brennan, J. (1993) Partitioning of fluorine and chlorine between apatite and aqueous fluids at high pressure and temperature: implications for the F and Cl content of high-*P*-*T* fluids. Earth and Planetary Science Letters, 17, 251–263.

Caciagli, N.C., and Manning, C.E. (2003) The solubility of calcite in water at 6–16 kbar and 500–800 °C. Contributions to Mineralogy and Petrology, 146, 275–285.

Cherniak, D.J., Pyle, J., and Rakovan, J. (2004) Synthesis of REE and Y phosphates by Pb-free flux methods and their utilization as standards for electron microprobe analysis and in design of monazite chemical U–Th–Pb dating protocol. American Mineralogist, 89, 1533–1539.

DeJong, G., and Williams, P.J. (1995) Giant metasomatic system formed during exhumation of mid-crustal Proterozoic rocks in the vicinity of the Cloncurry Fault, northern Queensland. Australian Journal of Earth Sciences, 42, 281–290.

Dunbar, N.W., Campbell, A.R., and Candela, P.A. (1996) Physical, chemical, and mineralogical evidence for magmatic fluid migration within the Capitan pluton, southeastern New Mexico. Geological Society of America Bulletin, 108, 318–333.

Ewing, R. (2001) The design and evaluation of nuclear-wasteforms: clues from mineralogy. Canadian Mineralogist, 39, 697–715.

Gao, J., John, T., Klemd, R., and Xiong, X. (2007) Mobilization of Ti-Nb-Ta during subduction: Evidence from rutile-bearing dehydration segregations and veins hosted in eclogite, Tianshan, NW China. Geochimica et Cosmochimica Acta, 71, 4974–4996.

Gieré, R. (1996) Formation of rare earth minerals in hydrothermal systems. In A.P. Jones, F. Wall, and C.T. Williams, Eds., Rare Earth Minerals, p. 105–150. Chapman and Hall.

Gratz, R., and Heinrich, W. (1997) Monazite-xenotime thermobarometry: Experimental calibration of the miscibility gap in the binary system $CePO_4$-YPO_4. American Mineralogist, 82, 772–780.

Hansen, E.C., Newton, R.C., Janardhan, A.S., and Lindenberg, S. (1995) Differentiation of late Archean crust in the eastern Dharwar Craton, Krishnagiri-Salem Area, South India. Journal of Geology, 103, 629–651.

Harlov, D.E. (2004) Fluid induced dehydration of the mafic lower crust from amphibolite to granulite facies: Nature and experiment. American Geophysical Union, Fall Meeting 2004, abstract V31A-1409.

——— (2011) Petrological and experimental application of REE- and actinide-bearing accessory minerals to the study of Precambrian high-grade gneiss terranes. Special Paper Geological Society of America Memoirs: Origin and Evolution of Precambrian High-Grade Gneiss Terrains, with Special Emphasis on the Limpopo Complex of Southern Africa pp. 13–24.

——— (2012) The potential role of fluids during regional granulite-facies dehydration in the lower crust. Geoscience Frontiers, 3, 813–827.

——— (2015) Apatite and fluids: A fingerprint for metasomatic processes. Elements, 11, 171–176.

Harlov, D.E., and Förster, H-J. (2002) High-grade fluid metasomatism on both local and a regional scale: the Seward Peninsula, Alaska, and the Val Strona Omegna, Ivrea-Verbano Zone, Northern Italy. Part II: phosphate mineral chemistry. Journal of Petrology, 43, 801–824.

——— (2003) Fluid-induced nucleation of (Y+REE)-phosphate minerals within fluorapatite: Nature and experiment. Part II. Fluorapatite: American Mineralogist, 88, 1209–1229.

Harlov, D.E., Hansen, E.C., and Bigler, C. (1998) Petrologic evidence for K-feldspar metasomatism in granulite facies rocks. Chemical Geology, 151, 373–386.

Harlov, D.E., Förster, H.-J., and Nijland, T.G. (2002) Fluid-induced nucleation of REE-phosphate minerals in fluorapatite: Nature and experiment Part I. Chlorapatite. American Mineralogist, 87, 245–261.

Harlov, D.E., Wirth, R., and Förster, H.-J. (2005) An experimental study of dissolution-reprecipitation in fluorapatite: fluid infiltration and the formation of monazite. Contributions to Mineralogy and Petrology, 150, 268–286.

Harlov, D., Tropper, P., Seifert, W., Nijland, T., and Förster, H.-J. (2006) Formation of Al-rich titanite ($CaTiSiO_4O$-$CaAlSiO_4OH$) reaction rims on ilmenite in metamorphic rocks as a function of f_{H_2O} and f_{O_2}. Lithos, 88, 72–84.

Harlov, D.E., Meighan, C.J., Kerr, I.D., and Samson, I.M. (2016) Mineralogy, chemistry, and fluid-aided evolution of the Pea Ridge Fe oxide-(Y+REE) deposit, southeast Missouri, USA. Economic Geology, 111, 1963–1984.

Harlow, G.E., and Davies, R. (2004) Status report on stability of K-rich phases at mantle conditions. Lithos, 77, 647–653.

Harrison, T.M., Catlos, E., and Montel, J.M. (2002) U-Th-Pb dating of phosphate minerals. Reviews in Mineralogy and Geochemistry, 48, 523–577.

Haschke, J.M. (1974) Structural relationships, crystal chemistry and anion substitu-

tion processes for M(III)X_3 systems of the lanthanides and actinides. Journal of Solid State Chemistry, 14, 238–246.

Ionov, D.A., and Hofmann, A.W. (1995) Nb-Ta-rich mantle amphiboles and micas: Implications for subduction-related metasomatic trace element fractionations. Earth and Planetary Science Letters, 131, 341–356.

Janots, E., Engi, M., Berger, A., Allaz, J., Schwarz, J.-O., and Spandler, C. (2008) Prograde metamorphic sequence of REE minerals in pelitic rocks of the Central Alps: implications for allanite-monazite-xenotime phase relations from 250 to 610 °C. Journal of Metamorphic Geology, 26, 509–526.

Janots, E., Engi, M., Rubatto, D., Berger, A., Gregory, C., and Rahn, M. (2009) Metamorphic rates in collisional orogeny from in situ allanite and monazite dating. Geology, 37, 11–14.

Kamenetsky, M.B., Sobolev, A.V., Kamenetsky, V.S., Maas, R., Danyushevsky, L.V., Thomas, R., Pokhilenko, N.P., and Sobolev, N.V. (2004) Kimberlite melts rich in alkali chlorides and carbonates; a potent metasomatic agent in the mantle. Geology, 32, 845–848.

Keppler, H. (2017) Fluids and trace element transport in subduction zones. American Mineralogist, 102, 5–20.

Klevtsova, R.F., and Klevtsov, P.V. (1965) Growth Forms and Crystal Structure of $YCl(OH)_2$. Soviet Physics Doklady, 10, 487.

Manning, C.E. (2004) The chemistry of subduction-zone fluids. Earth and Planetary Science Letters, 223, 1–16.

Markl, G., and Piazolo, S. (1998) Halogen-bearing minerals in syenites and high-grade marbles of Dronning Maud Land, Antarctica: monitors of fluid compositional changes during late-magmatic fluid-rock interaction processes. Contributions to Mineralogy and Petrology, 132, 246–268.

Markl, G., Ferry, J.M., and Bucher, K. (1998) Formation of saline brines and salt in the lower crust by hydration reactions in partially retrogressed granulites from the Lofoten Islands, Norway. American Journal of Science, 298, 705–757.

Mayanovic, R.A., Anderson, A.J., Basset, W.A., and Chou, I.M. (2009) Steric hindrance and the enhanced stability of light rare-earth elements in hydrothermal fluids. American Mineralogist, 94, 1487–1490.

Montel, J.M. (1993) A model for monazite/melt equilibrium and application to the generation of granitic magmas. Chemical Geology, 110, 127–146.

Newton, R.C., and Manning, C.E. (2002) Experimental determination of calcite solubility in H_2O-NaCl solutions at deep crust/upper mantle pressures and temperatures: implications for metasomatic processes in shear zones. American Mineralogist, 87, 1401–1409.

——— (2005) Solubility of anhydrite, $CaSO_4$, in NaCl-H_2O solutions at high pressures and temperatures: applications to fluid-rock interaction. Journal of Petrology, 46, 701–716.

——— (2006) Solubilities of corundum, wollastonite and quartz in H_2O-NaCl solutions at 800°C and 10 kbar: Interaction of simple minerals with brines at high pressure and temperature. Geochimica et Cosmochimica Acta, 70, 5571–5582.

——— (2010) Role of saline fluids in deep-crustal and upper-mantle metasomatism: insights from experimental studies. Geofluids, 10, 58–72.

Newton, R.C., Aranovich, L.Y., Hansen, E.C., and Vandenheuvel, B.A. (1998) Hypersaline fluids in Precambrian deep-crustal metamorphism. Precambrian Research, 91, 41–63.

Pan, Y., and Fleet, M.E. (1996) Rare element mobility during prograde granulite facies metamorphism: significance of fluorine. Contributions to Mineralogy and Petrology, 123, 251–262.

Pasteris, J.D., Harris, T.N., and Sassari, D.C. (1995) Interactions of mixed volatile-brine fluids in rocks of the southwestern footwall of the Duluth Complex, Minnesota—evidence from aqueous fluid inclusions. American Journal of Science, 295, 125–172.

Philippot, P., and Selverstone, J. (1991) Trace element-rich brines in eclogitic veins: implications for fluid compositions and transport during subduction. Contributions to Mineralogy and Petrology, 106, 417–430.

Philippot, P., Chevallier, P., Chopin, C., and Dubessy, J. (1995) Fluid composition and evolution in coesite-bearing rocks (Dora Maira massif, western Alpa): implications for element recycling during subduction. Contributions to Mineralogy and Petrology, 121, 29–41.

Reed, M.J., Candela, P.A., and Piccoli, P.M. (2000) The distribution of rare earth elements between monzogranitic melt and the aqueous volatile phase in experimental investigations at 800 °C and 200 MPa. Contributions to Mineralogy and Petrology, 140, 251–262.

Rubatto, D., and Hermann, J. (2003) Zircon formation during fluid circulation in eclogites (Monviso, Western Alps): implications for Zr and Hf budget in subduction zones. Geochimica et Cosmochimica Acta, 67, 2173–2187.

Safonov, O.G., Kovaleva, E.I., Kosova, S.A., Rajesh, H.M., Belyanin, G.A., Golunova, M.A., and Van Reenen, D.D. (2012) Experimental and petrological constraints on local-scale interaction of biotite-amphibole gneiss with H_2O-CO_2-(K, Na)Cl fluids at middle-crustal conditions: Example from the Limpopo Complex, South Africa. Geoscience Frontiers, 3, 829–841.

Sampson, I.M., Liu, W., and Williams-Jones, A.E. (1995) The nature of orthomagmatic fluids in the Oka carbonatite, Quebec, Canada: evidence from fluid inclusions. Geochimica et Cosmochimica Acta, 59, 1963–1977.

Schmidt, C., Rickers, K., Bilderback, D.H., and Huang, R. (2007) In situ synchrotron radiation XRF study of REE phosphate dissolution in aqueous fluids to 800°C. Lithos, 95, 87–102.

Shmulovich, K.I., Yardley, B.W.D., and Graham, C.M. (2005) The solubility of quartz in chloride solutions at 400°–800°C and 0.1–0.9 GPa. Goldschmidt Conference Abstract 2005, abstract V69A-823.

Spear, F.S., and Pyle, J.M. (2002) Apatite, monazite and xenotime in metamorphic rocks. Reviews in Mineralogy and Geochemistry, 48, 293–335.

Taghipour, S., Kananian, A., Harlov, D., and Oberhänsli, R. (2015) Kiruna-type iron oxide-apatite deposits, Bafq district, central Iran: fluid-aided genesis of fluorapatite-monazite-xenotime assemblages. Canadian Mineralogist, 53, 479–496.

Todd, C.S., and Evans, B.W. (1994) Properties of CO_2-induced dehydration of amphibolite. Journal of Petrology, 35, 1213–1240.

Tomlinson, E., Jones, A., and Milledge, J. (2004) High-pressure experimental growth of diamond using C–K_2CO_3–KCl as an analogue for Cl-bearing carbonate fluid. Lithos, 77, 287–294.

Touret, J.L.R. (1985) Fluid regime in southern Norway: the record of fluid inclusions. In A.C. Tobi and J.R.L. Touret, Eds., The Deep Proterozoic Crust in the North Atlantic Provinces, p. 517–549. Reidel, Dordrecht.

Touret, J.L.R., and Nijland, T.G. (2013) Metasomatism and the Chemical Transformation of Rock. The Role of Fluids in Terrestrial and Extraterrestrial Processes. Part of the series Lecture Notes in Earth System Sciences, p. 415–469. Springer.

Tropper, P., and Manning, C.E. (2005) Very low solubility of rutile in H_2O at high pressure and temperature, and its implications for Ti-mobility in subduction zones. American Mineralogist, 90, 502–505.

——— (2007a) The solubility of fluorite in H_2O and H_2O-NaCl at high pressure and temperature. Chemical Geology, 242, 299–306.

——— (2007b) The solubility of corundum in H_2O at high pressure and temperature and its implications for Al mobility in the deep crust and upper mantle. Chemical Geology, 240, 54–60.

Tropper, P., Manning, C.E., and Harlov, D.E. (2011) Solubility of $CePO_4$ monazite and YPO_4 xenotime in H_2O and H_2O-NaCl at 800°C and 1 GPa: implications for REE and Y transport during high-grade metamorphism. Chemical Geology, 282, 58–66.

——— (2013) Solubility of $CePO_4$ monazite and YPO_4 xenotime in H_2O-NaF at 800°C and 1 GPa. Geofluids, 13, 372–380.

Williams-Jones, A.E., Migdisov, A.A., and Samson, I.M. (2012) Hydrothermal mobilization of the REE—a tale of ceria and yttria. Elements, 8, 355–360.

Yang, X.-M., Yang, X.-Y., Zheng, Y.-F., and Le Bas, M.J. (2003) A rare earth element-rich carbonatite dyke at Bayan Obo, Inner Mongolia, North China. Mineralogy and Petrology, 78, 93–110.

Yardley, B.W.D. (1985) Apatite composition and the fugacities of HF and HCl in metamorphic fluids. Mineralogical Magazine, 49, 77–79.

Yardley, B.W.D., and Graham, J.T. (2002) The origins of salinity in metamorphic fluids Geofluids, 2, 249–256.

Zhuravleva, M., Stand, L., Wei, H., Hobbs, C., Boatner, L.A., Ramey, J.O., Shah, K., Burger, A., Rowe, E., Bhattacharya, P., and others. (2013) Hygroscopicity evaluation of halide scintillators. Nuclear Science Symposium and Medical Imaging Conference (NSS/MIC), 2013 IEEE.

Manuscript received April 25, 2017
Manuscript accepted July 28, 2017
Manuscript handled by Don Baker